School of Mechanical, Aerospace & Automotive Engineering
Faculty of Engineering, Environment and Computing
Coventry, United Kingdom

Stress and Dynamic

Written by

Ravi Chaudhary, 10947986

Contents

List of Figures

Experimental Modal Analysis of a Structural Component with Model Validation

Introduction

Modal analysis provides insight into the vibration of complex mechanical structures when excited by a load or a force. The dynamics of the structure are described in terms of its modal parameters comprising of mode shapes, damping factors and natural frequencies based on Frequency Response Function measurements **(Crystal Instruments, n.d.)**, which denotes the relationship between the excitation and the response from both time and frequency domains:

$$FRF = \frac{Vibration\ (output)}{Force\ (input)}$$

These modal parameters collectively make up the mathematical modal model, which is a more accurate representation of the dynamic properties of the structure **(He & Fu, 2001)**. Performing modal analysis allows the engineer to understand the vibrations of each mode shape thus, conducting experiments provides engineers the knowledge needed to optimise their mechanical designs. Essentially, this involves changing a complex structure with multiple degrees of freedom into a set decoupled single degree of freedom systems.

Conducting this experiment was approached through artificially applying an impulsive force at various defined nodes by using an impact hammer, to derive the modal model from an assumed linear time-invariant system. This method is known as impact-hammer testing. The excitation is measured from a force transducer, with the response measured by the accelerometer. Both signals were computed into an analyser that computed the FRF data, which was then analysed to identify the modal parameters for the mechanical structure. Modal testing is extensively used in a variety of industries, such as automotive and aerospace, to modify and optimise structural designs, thus decreasing the impact of applied forces most notably through the aid of Finite Element Analysis (FEA).

Considering the theory of the topic, it is expected for the vibrations on each mode shape to vary depending on the impulse forces imposed on the various sections of the structure, along with the magnitude of the force impacting the oscillations in the system.

A. EXPERIMENTAL METHODOLOGY

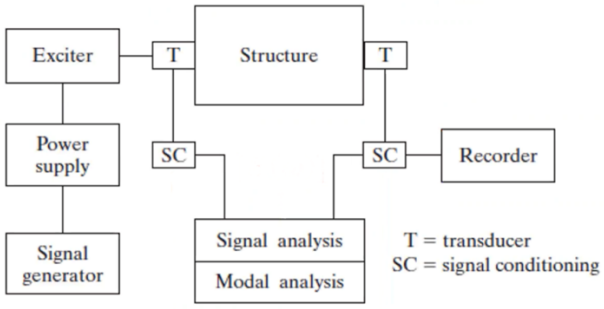

Figure 1.1: A diagram of the apparatus (Coventry University, 2023)

Figure 13.1 shows how the various components formed a network to make this experiment feasible. All components included were connected for the focal point of the structure due to the nature of what is being measured – modal vibration. A cubic structure **(figure 14.2)** is suspended from a wire rigged onto a wooden frame. Two transducers are connected to the structure: one input and one output. Signal conditioning is applied to the transducers, to eliminate any unwanted noise from the analogue signals emitted from the experiment. With this, it will be much easier to measure the signals required.

The structure mentioned above is shown in figure 2 as high-tensile cubic-shaped material suspended with a bungee cord in a wooden frame. It had nodes labelled from 1-28 to mark the points of impact for the hammer, with node 21 being occupied by the accelerometer. Being hung allowed free vibration of the material but not restricting its lateral movement. It is important to note that the geometry and dimensions being all the same, along with the nodes being symmetrical across all 4 faces of the model.

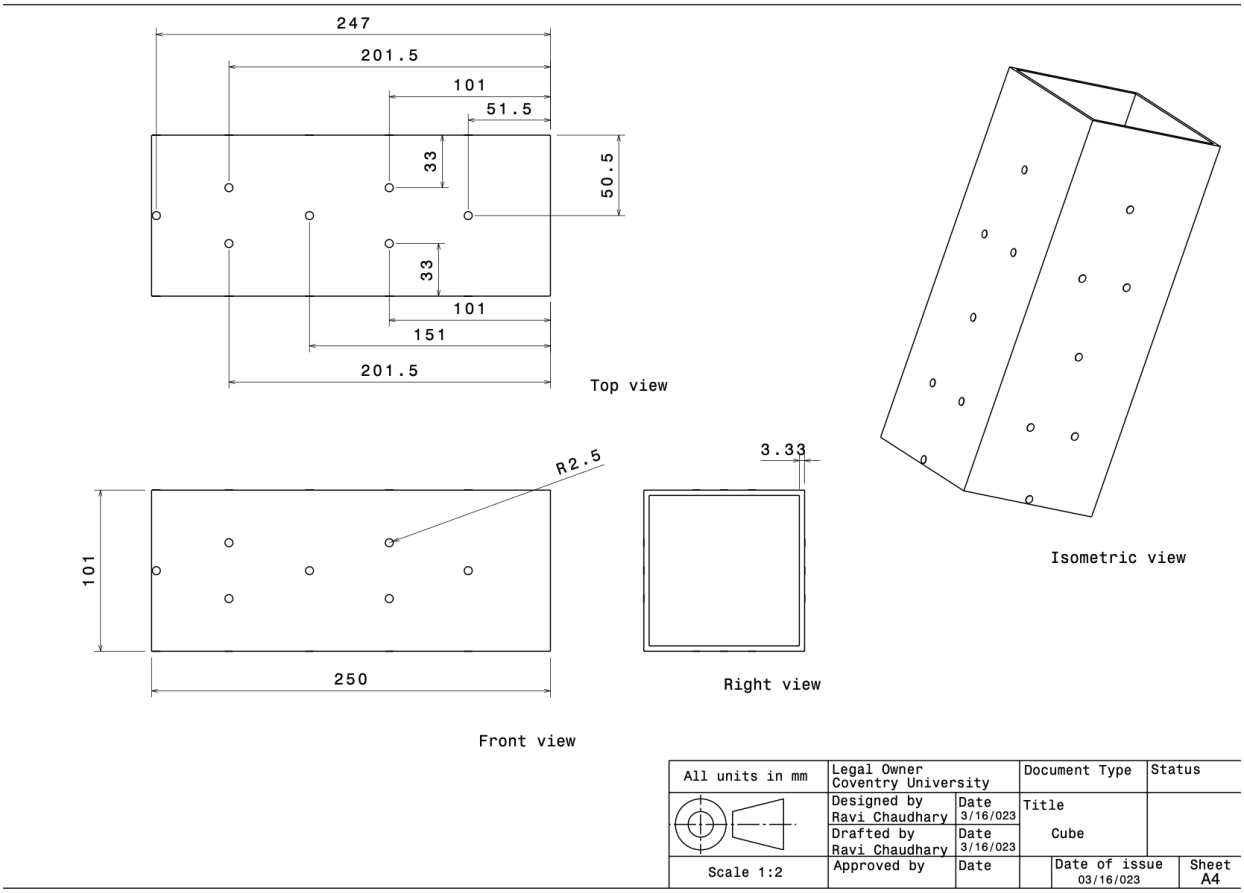

Figure 2.2: Illustration of the mechanical model, with geometry

Recorder (Laptop):

A computer was used to record the results using MATLAB Signal Analyser. Specifically, the results derived from the lab experiment were a graph showing the impact of the strike, a graph showing the movement of the specified node, as well as the FFT graphs for each given mode shape.

Signal Generator:

It was included to create electronic signals to allow the data to be recorded and transformed.

Transducers:

Two transducers are connected to the structure. 1 input and 1 output. The input (hammer) is measured for force and the output (accelerometer) is measured for acceleration thus the change in vibration intensity.

Hammer:

The modal hammer is an exciter. Instrumented with a load cell at the tip, it is installed with a crystal inside to transform the tip deformation into an electrical charge. The mass can be changed, which affects the forces behind each strike – a heavier hammer means a higher force. Tips can be changed according to the characteristics and dimensions of each structure.

Accelerometer:

This device measures vibration in the x, y and z axes. A cable is attached to the accelerometer and splits into 3, with each axis being assigned its cable, thus recording each individually. It is important to note that the accelerometer was connected to node 21.

Data setup:

There are 4 channels Upon impact of the hammer, the electrical charge generated from the modal hammer's load cell is amplified and measured by this device. To measure the data, it is converted to voltage difference (mV).

Inputting specified parameters into the software prior to performing the procedure guaranteed that the outputs and FE simulations were obtained and carried out accurately. The acquisition box possesses 4 channels, with the impact hammer imputed into channel 2, and the accelerometer into channel 1 with both of their sensitivities allocated.

Table 1.1: Data of the Shear Accelerometer.

Name	Shear Accelerometer
Model	353B33
Sensitivity	100 mV/g

Table 2.2: Data of the Impulse Force Hammer.

Name	Impulse Force Hammer
Model	086C03
Sensitivity	2.234 mV/N

Upon the impact of the hammer, the electrical charge generated from the modal hammer's load cell is amplified and measured by the acquisition box. To measure the data, it is converted to voltage difference (mV). Furthermore, it was test time was set to 4 seconds using acquisition box, in order to sufficiently capture data according to the resolution of the Frequency Response Model.

Procedure (FIRST DRAFT)

1. After pre-processing the data inputs, identify the various planes according to the direction the hammer will be striking x, y, -x, -y all have 7 nodes each. The nodes are labelled 1-28.

2. Using the impact hammer, lightly and sharply strike the nodes. This should be carried out, after clicking ‘record’, as a test run initially with 2-3 trials to verify the functionality of the software.
3. Click ‘record’ on MATLAB before collecting the data obtained from the hammer strike.
4. After this, lightly and sharply strike node 1, ensuring to extract the hammer immediately after impact to avoid unintentional double strikes. Double impacts are ruled as bad strikes due to multiple strikes on the
5. Upon impact, the load cell inside the hammer transforms the deformation of the tip into an electrical charge, which is amplified by the acquisition box.
6. The data acquisition box will receive the signals from the hammer and accelerometer and process them into data to be computed in MATLAB, with the acquisition time set to 4s.
7. The data acquisition box was setup to read the data for 4 seconds. After striking, wait 4 seconds for the pitcher to be refreshed.
8. Open ‘Signal Analyser’, to read and record the time data.
9. Repeat this for the rest of the nodes, except node 21.

Data Pre-processing:

Data pre-processing involves frequency-response functions for modal analysis.

FRFs tools are useful to determine a system's frequency response functions based on measured input and output data. FRFs are crucial in structural dynamics and vibration analysis as it shows how the system behaves at various frequencies. Approximating FRFs helps to identify natural frequencies, damping ratios, and mode shapes of the structure—all crucial information for comprehending its dynamic behaviour and analyse vibration.

The "modalfrf" function used in the MATLAB code returns the outputs named: "FRFs", "f", and "cohs". "FRFs" is the system's response at each frequency of the input, "f" is a frequency vector points in the response function, and "cohs" is the coherence matrix that shows the correlation between input and output measurements at each frequency point. The code also provides options for specifying different measurement configurations, estimators, and sensors, which is useful to analyse different types of systems and experimental setups (MathWorks, modalfrf, n.d.).

Windowing: The “winlen” variable in the MATLAB code for data pre-processing denotes the length of the frame that was used for the FRF analysis. Both the input force (frc) and the output response (rsp) signals are subject to this window's application. The windowing function used is the rectangular window denotes each data segment is multiplied by a rectangular window of length “winlen”. The number of frequency bins used for the FRF analysis is indicated by the nbins variable, which is derived from the “winlen” variable **(MATLAB).**

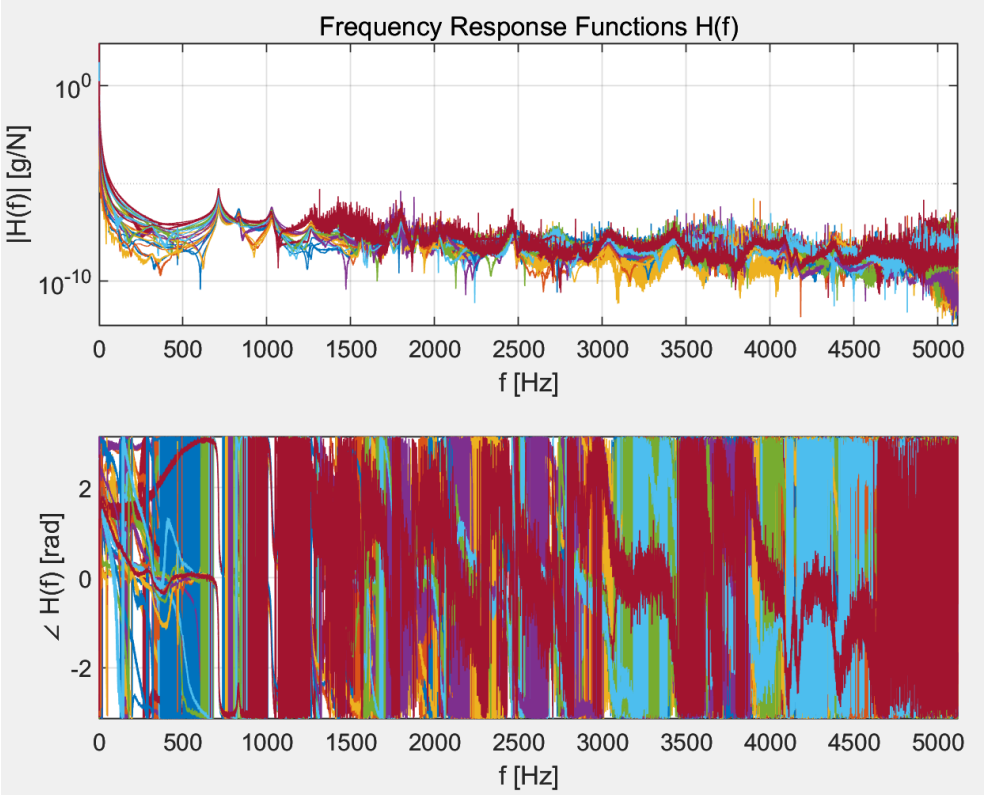

Figure 3.3: Frequency Response Function H(F).

Figure 15.3 shows, the frequency response functions where the parameter "Estimator" is used in MATLAB, specifying the H2 estimator which has been used to calculate the FRFs. The frequency responses of all 28 strikes on the individual nodes has been captured and shown in one graph.

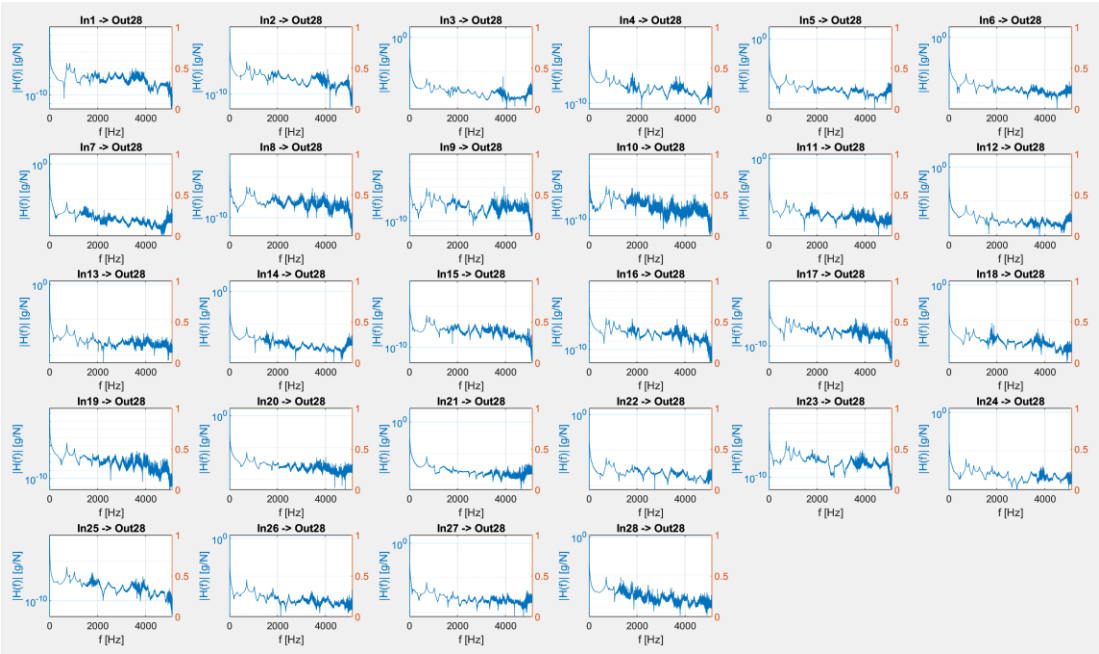

Figure 4.4: Frequency response functions obtained from 28 strikes.

Figure 16.4 shows the frequency response functions of 28 strikes on 28 individual nodes. The graphs are shown separate for each strike on the each node, it is easier to read the FRFs. The FRFs graph shows the good range of peaks and also has quite a lot of disturbances in some of the strikes after certain frequencies.

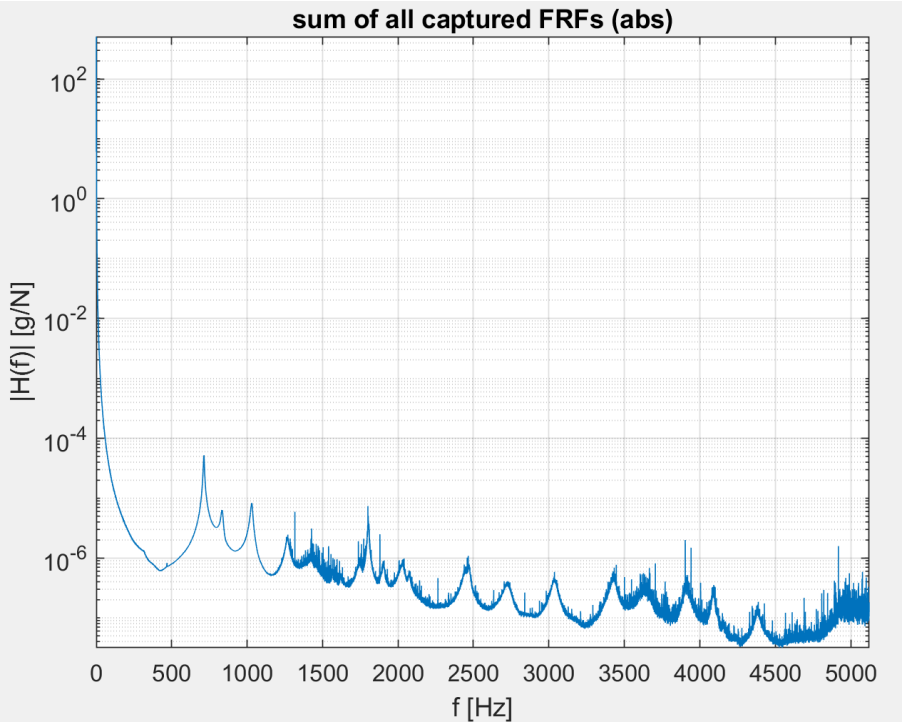

Figure 5.5: Sum of all captured FRFs.

All the higher peaks to lower peaks from 28 strikes at 28 different nodes is sum up and resulted as can be seen in **fig 17.5**. Due to this addition of peaks, the smaller peaks which are invisible in the individual frequency response graphs has been appeared. The sharper and the higher peaks can be achieved due to addition of all FRFs. Similarly, there certain disturbances around the frequency 1500 Hz and after 3500 Hz.

Extraction Algorithms**:**

It includes the stabilization diagram for modal analysis. The least-squares complex exponential (LSCE) method is used by "modalsd" to create the diagram and determine the natural frequencies and damping ratios for modes ranging from 1 to 50. A frequency vector 'f' consists of many elements as the same number of rows in a FRFs. This illustration in the diagram can be used to distinguish between computational and physical modes **(MathWorks, MathWorks, n.d.).**

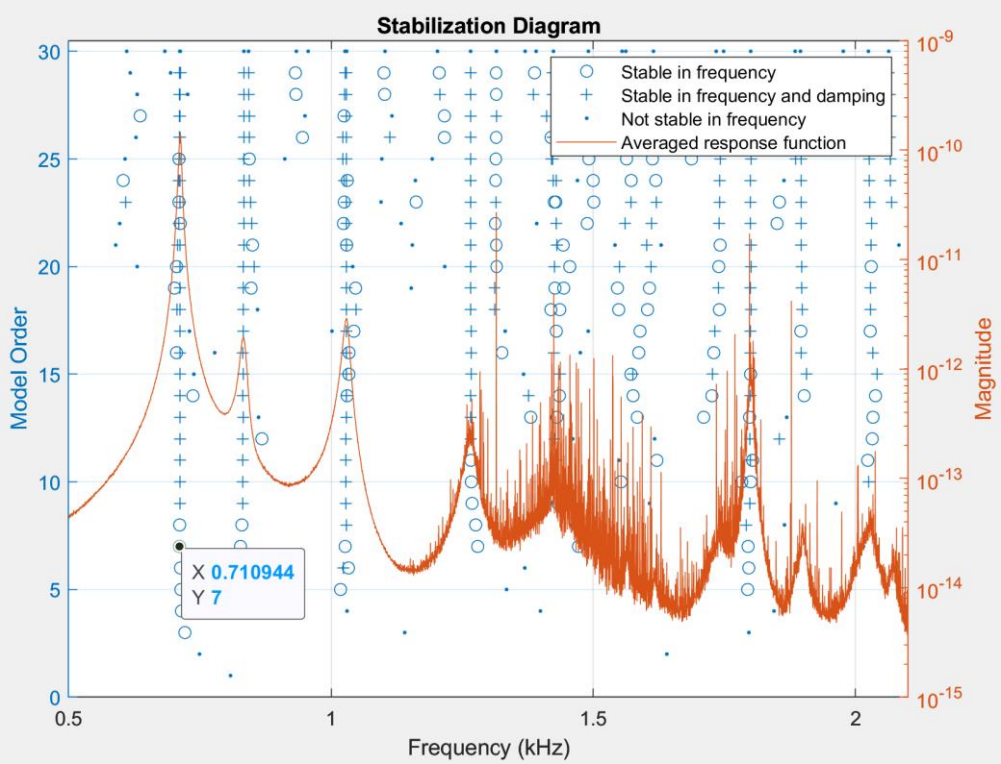

Figure 6.6: Stabilization of Diagram of Modal Analysis.

Fig 18.6 shows the stabilization diagram of 30 physical modes to identify. To limit the stability criteria, the pole with stable frequency has been chosen i.e., (0.710944, 7). The natural frequency of the chosen pole can be called stable because the variation is less than 0.01%.

Bandwidth: The computation has been repeated using the least square computational exponential algorithm. Looking at all the stable poles and higher peak response, the frequency range has been restricted in between 500 HZ to 2100 Hz. The 5 physical modes are extracted using the stability diagram for the analysis and the modes selected are 1, 2, 3, 4 and 6 **(MathWorks, n.d.).**

Data Validation:

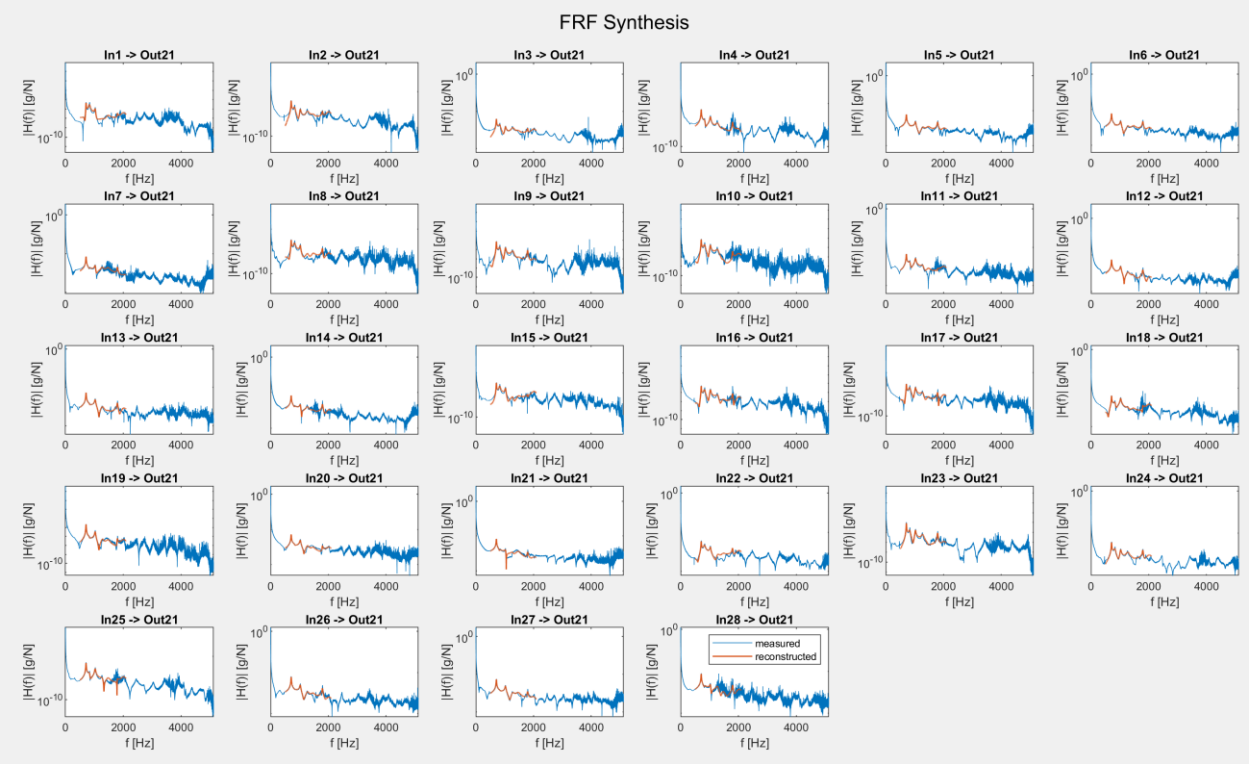

Figure 7.7: Frequency response Functions synthesis.

Fig 19.7 shows the frequency response function synthesis of the measured and the regenerated value which makes it feasible to see how accurately the estimated value/regenerated value replicates the dynamics of the physical structure.

The least-squares complex exponential (LSCE) method is used to calculate the modal parameters. The 5 physical mode frequencies are derived from the stabilisation diagram and is define to a model order of 26 modes. For each input reference, the function produces a unique collection of natural frequencies and damping ratios. After that, the regenerated frequency response functions are compared to the measured one and are plotted. Since, the frequency range has been restricted in between 500 HZ to 2100 Hz, the value is regenerated within that frequency range and the results show the better peaks than the measured ones in most of the modes as can be seen in **Figurev19.7**.

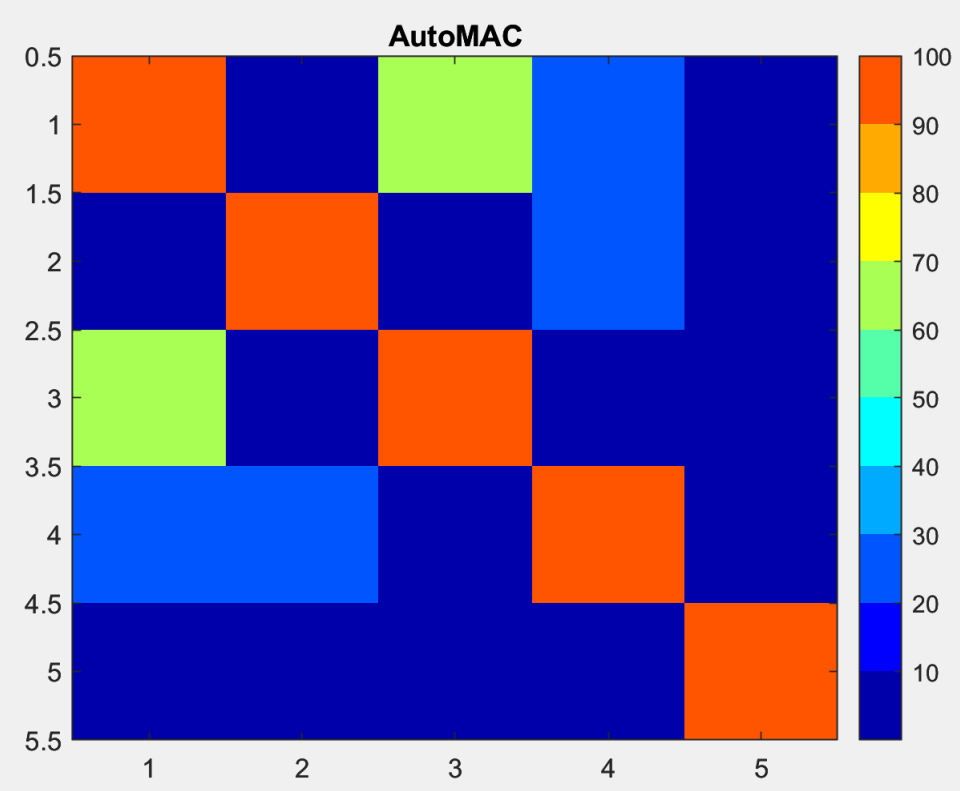

Figure 8.8:Stabilization Diagram of Modal Analysis.

In the above figure, the AutoMAC was used to compare the mode shapes of itself. As the 5 modes shapes were extracted during the frequency stabilization process, it has been compared to itself to determine the mode shape similarities forming [5x5] matrix Since, it is compared to itself all the mode shapes in the diagonal are similar and has 100% similarity. The mode shape 1 and the mode shape 2 has only 10% similarities whereas the mode shape 1 and 3 shows 70% similar vibration. The mode shape 1 and the mode shape 4 resembles 40% similarity and the mode shapes 1 with the mode shape 5 is very dissimilar with only 10% similarities in the way of their vibration.

Experimental results:

The identified natural frequencies for the 5 mode shapes respectively shapes are:

Identified natural frequencies:

1. 710.9 Hz
2. 827.1 Hz
3. 1026.5 Hz
4. 1279.0 Hz
5. 1795.1 Hz

Identified Damping ratios:

The identified damping ratios for 5 mode shapes are:

1. 0.0049
2. 0.0249
3. 0.0116
4. 0.0292
5. 0.0048

Modal Shapes results:

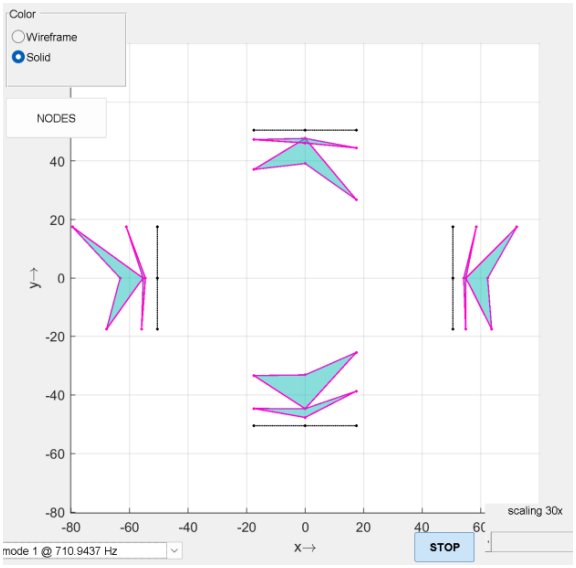

Figure 9.9:Modal shape at frequency 710.94 Hz Hz.

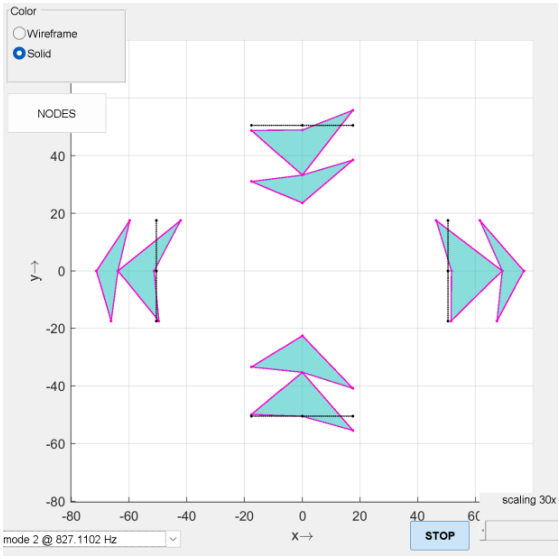

Figure 10.10:Modal shape at frequency 827.11

The frequency at 710.94 Hz and 827.11 Hz resembles very similar mode shapes but the difference is the side of vibration where in mode shape1, the top edge is fixed and the bottom is vibrating and in the mode shape 2, the top edge is vibrating, and the bottom is fixed. It is because in the case of mode shape 1, the bottom edge is free to vibrate whereas the top edge was pinched with the bungee cord. This has created the asymmetricity. Since, they should most likely be vibrated at the same time but due to one side being pinched the top edge vibrates later in the mode shape 2.

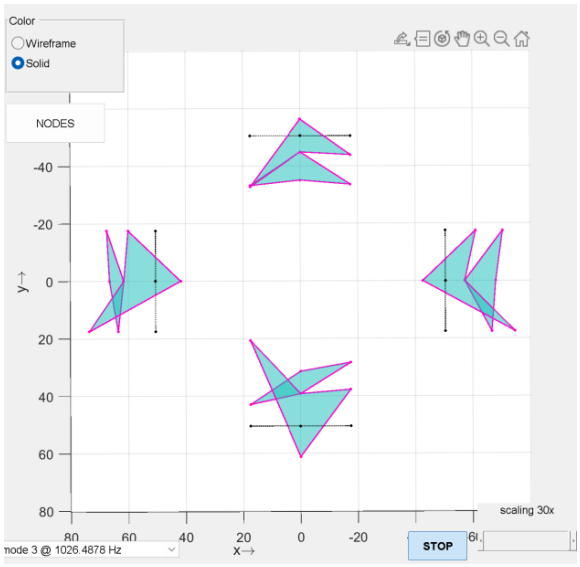

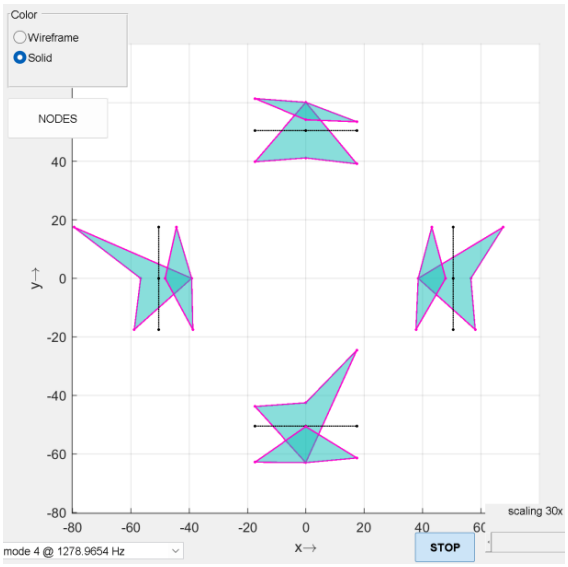

Figure 11.11:Modal shape at frequency 1026.48 Hz. *Figure 12.12:Modal shape at frequency 1278.96 Hz.*

The mode shape at frequency 1026.48 Hz is 70% similar with mode shape 1 as resulted using MAC. Here at the frequency 1025.48, the top edge or node of two sides facing opposite to each other are contracting, at the same time expansion on the top edge on the other two sides of the prism can be seen. While first two sides top edge described are contracting, there is small expansion in the bottom edge can be observed and the other two sides experiencing expansion at the top has a contraction at the bottom edge.

The mode shape at frequency 1278.96 Hz is 40% similar with mode shape 1 as resulted using MAC. It can be observed from fig 10, the middle node of the prisms are highly subjected to contraction and expansion. When the middle node of two sides facing opposite to each other contracts, the other two faces expand. At the same time the small expansion at the top and bottom of the first two faces described can be seen and the small contraction at the top and bottom edge of the other two faces described can be seen can be observed.

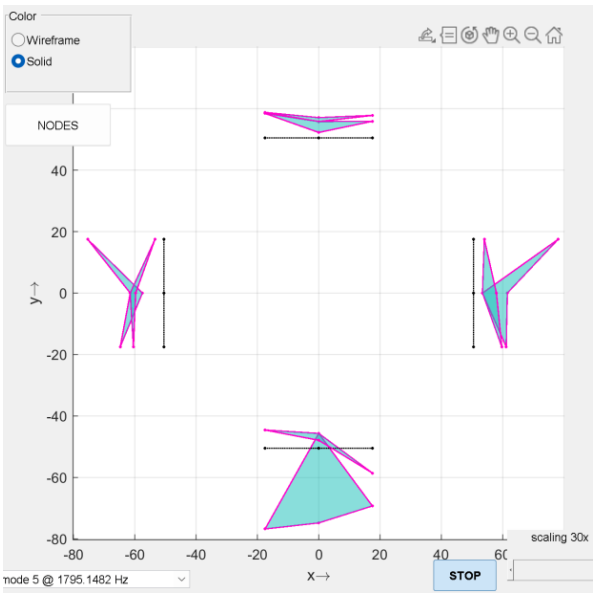

Figure 13.13:: Modal shape at frequency 1795.14 Hz.

The mode shape at frequency 1795.14 Hz is 10% similar with mode shape 1 as resulted using MAC. It shows the contraction and expansion of all the sides together. The middle nodes of all the sides are highly in contraction which is contracting the top and the bottom edge where no expansion can be seen at the same time. After contraction, there is an expansion of all the four sides together where the corners are barely affected.

B. Mathematical (FE) model:

The mathematical analysis was performed in a software Abacus. The analysis begins from making a 3D model of a prism shape which was imported to the software, Abacus. The material of the prism used during the experiment was identified calculating the density of the material using the measured mass of a prism (848 gm) and the volume extracted using CAD software. The density was found to be 2.87e-9 tons/mm^3 which was utilised to identify the material using software, GRANTA EDUPACK. The property found resembles to the material to be Aluminium. The lowest young's modulus value of the Aluminium was considered for the analysis. The mesh was created, and the mesh convergence study has been done with different element sizes and nodes. The step was created in the **solution step** where the frequency is chosen as a type to study the modal shapes of the material at different frequencies. The solver was chosen to be Lanczos Eigen solver. The 26 number of modes were selected for analysis where the first 6 modes are the rigid modes, and the rest 20 modes are the elastic modes. The first 6 modes are always the rigid modes in the free-free analysis as in this experiment. The job was created and was submitted to extract the results.

The loads and the boundary conditions weren't considered in this mathematical approach. It is because the free-free analysis is based on the concept of free vibration which is possible only when the structure is allowed to vibrate without subjected to any external excitations and constraints. Similarly, in free-free analysis, the stiffness matrix is assumed to be unaffected by external disturbances and boundary conditions assuming the structure can vibrate freely in all directions. However, the stiffness matrix can be applied to determine structure response due to external excitations after the natural frequencies and mode shapes of the structure are determined.

The element type for the mesh was chosen to be "quadratic" and the shape is chosen as "hexahedral" for all the mesh convergence studies. It is because in 3D FE analysis, the quadratic element type increases the accuracy in the results providing precise and effective modelling of complicated geometries. Similarly, in comparison to linear elements, quadratic elements have more nodes and degrees of freedom. Consequently, they can more accurately represent the curvature and non-linearities of the issue under consideration.

The mesh convergence study was done with different element sizes and nodes. The result in the frequencies with different number of nodes are tabulated in **table 5.3.** The first five frequencies after the rigid modal shapes are considered for the mesh convergence study. The study was done 7 time with different number of nodes for the convergence. The convergence of the frequencies with the increased number of nodes can be observed, still little difference in the decimal values can be seen. It suggested that the convergence hasn't been fully met. Further convergence study with increased number of nodes might improve the result but the student version of Abacus used for this analysis constricts with certain number of nodes. Therefore, the frequency results with the highest number of

nodes used i.e., 244350 was used for the further analysis of modal shapes and comparison with the experimental results.

Convergence table:

Table 3.3: Mesh convergence study.

S.N	Element sizes	Number of nodes	First five frequencies after rigid modal shapes
1.	20640	99244	i. 476.18 ii. 505.56 iii. 802.13 iv. 902.65 v. 1219.3
2.	33040	158592	i. 475.50 ii. 504.93 iii. 802.12 iv. 902.56 v. 1219.0
3.	39040	187148	i. 475.43 ii. 504.87 iii. 802.12 iv. 902.55 v. 1219.0
4.	42840	205254	i. 475.37 ii. 504.82 iii. 802.12 iv. 902.54 v. 1219.0
5.	46920	224802	i. 475.20 ii. 504.66 iii. 802.12 iv. 902.52 v. 1218.9
6.	50320	241092	i. 475.07 ii. 504.54 iii. 802.12 iv. 902.51 v. 1218.9
7.	51000	244350	i. 475.04 ii. 504.52 iii. 802.12 iv. 902.50 v. 1218.8

Convergence Graph:

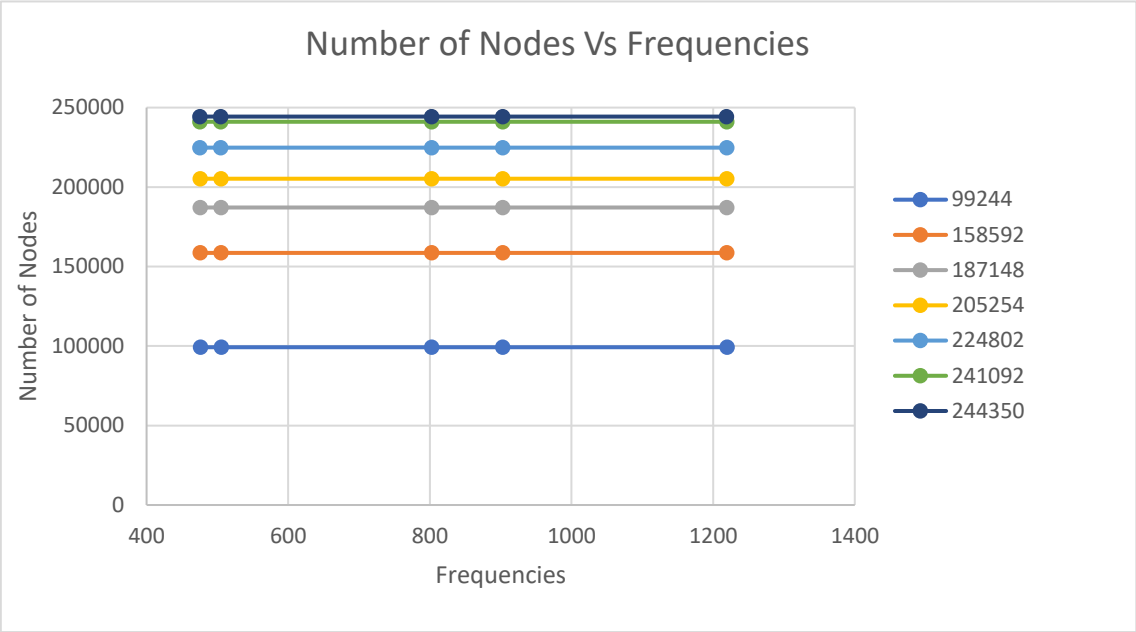

Figure 14.14:Convergence graph showing nodes Vs Frequency.

The **fig 26.14** shows the convergence graph of Number of nodes Vs Frequencies where the first five frequencies after the rigid modal shapes of difference node numbers has been compared. Due to very small difference in the frequencies with the different number of nodes used for convergence, the frequencies in the graphs at each nodes look very similar but there is small difference of decimal values. The line with the number of nodes, 244350 has the most converged frequency values in comparison to the rest.

Results:

The pictures below are the results of mode shapes at different frequencies which resembles very similar mode shapes obtained from the experimental analysis.

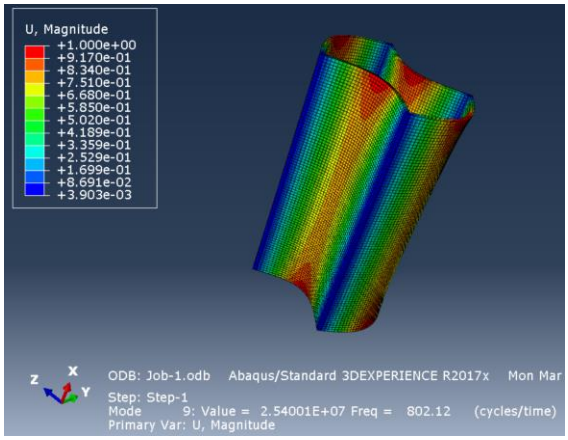

Figure 15.15:Mode shape at frequency 802.12 Hz.

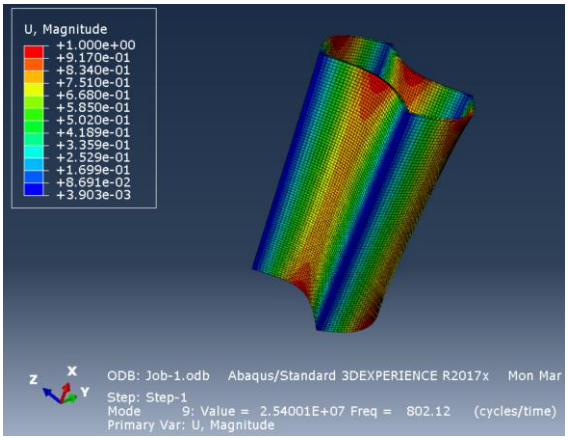

Figure 16.15:Mode shape at frequency 802.12 Hz.

The modal shape analysis shown in the fig **27.15** and **fig 15** are same. It is because the modal shape at frequency of 802.12 Hz in the theoretical analysis resembles the two mode shapes i.e., mode shape 1 and mode shape 2 of the experimental analysis.

The modal shape at frequency 802.12 Hz shows the alternate contraction and expansion of the four sides of the prism (2 sides each). When the two sides of opposite faces contracts, another two sides of opposite faces expand together.

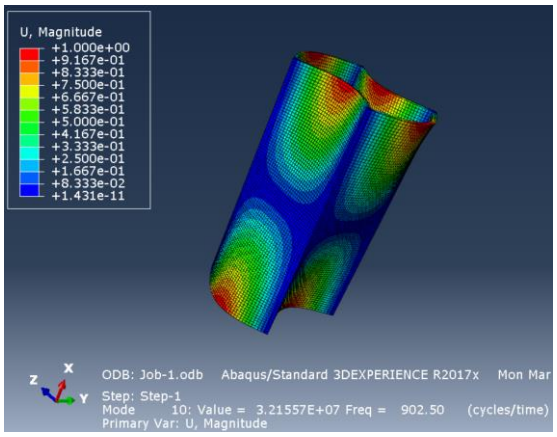

Figure 17.16:Mode shape at frequency 902.50 Hz.

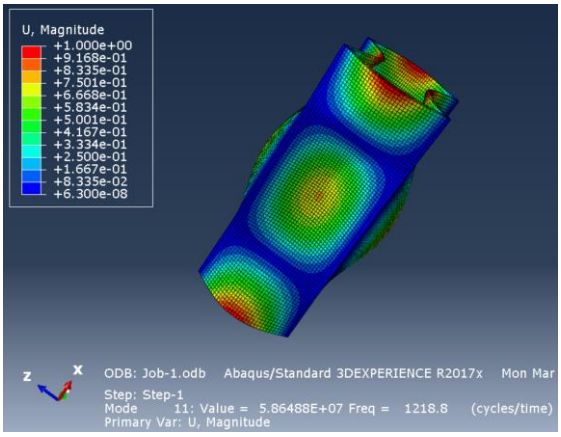

Figure 18.17:Mode shape at frequency 1218.8 Hz.

The mode shape at frequency 902.50 Hz resembles the top edge of the two sides facing opposite to each other contracts and the bottom edge has a small expansion whereas the other two sides facing opposite to each other has an expansion at the top edge and the contraction at the bottom at the same time.

The mode shape at the frequency of 1218.8 Hz shows the contraction of middle section of prism or the nodes of the two sides facing opposite to each other and has the expansion of at the top and

bottom edges whereas, the other two sides facing opposite to each other has an expansion in the middle and has the contraction on the top and bottom of the edges.

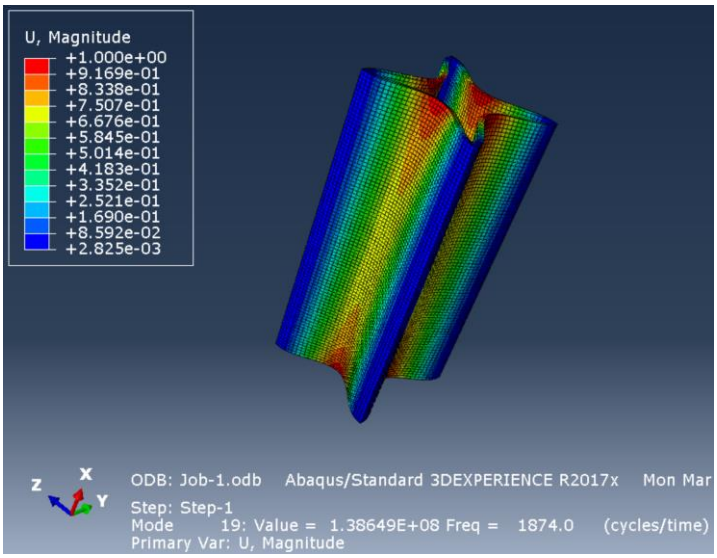

Figure 19.18:Mode shape at frequency 1874.0 Hz.

The mode shape in the **fig 31.18** shows the contraction of all the four sides of the prism at the same time. Similarly, there will be the expansion of all the sides of the prism together after contraction. The contraction and expansion of all the sides keeps going on while all the four corners remain unaffected.

C. Model Validation:

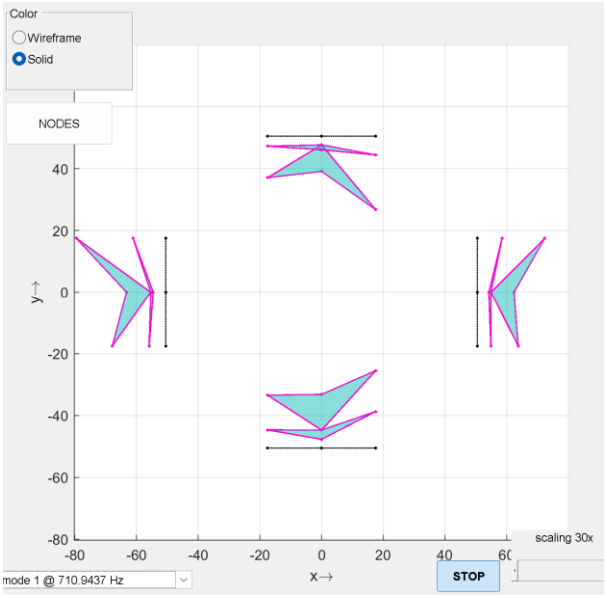

Figure 20.19:Mode shape at frequency 710.94 Hz. Hz. (Experimental Analysis)

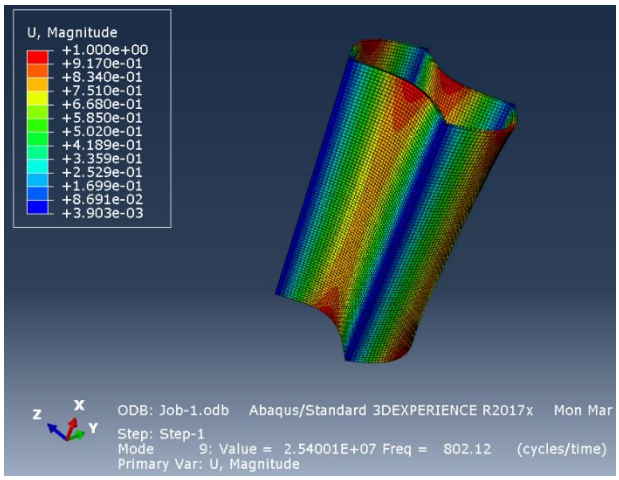

Figure 21.20:Mode shape at frequency 802.12 (Theoretical Analysis).

Since, the mode shapes of experimental and theoretical analysis at the frequency 710.94 Hz and 802.12 Hz are similar respectively. The percentage error considering their frequencies has been calculated.

Percentage Error

$$\frac{802.12-710.94}{802.12} * 100\% = 11.36\%$$

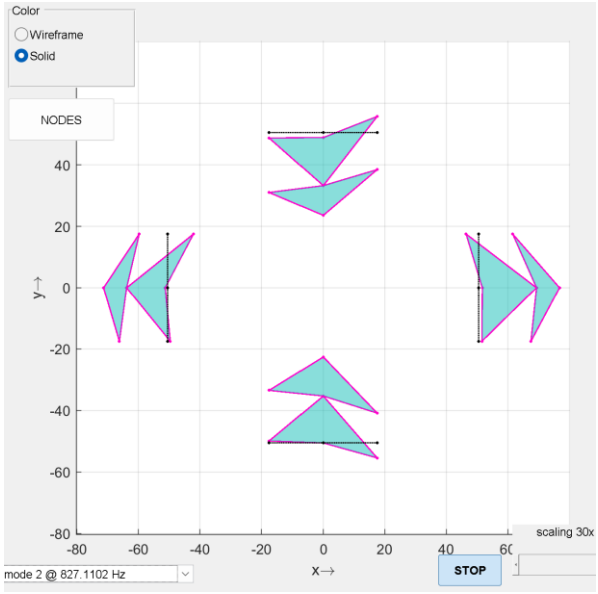

Figure 22.21:Modal shape at frequency 827.11 HZ. Hz. (Experimental Analysis).

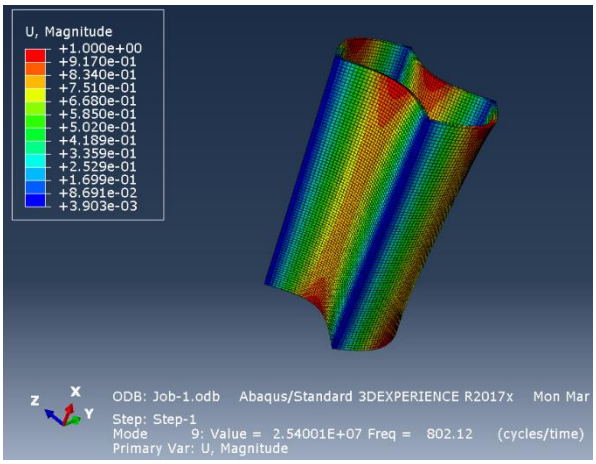

Figure 23.22:Mode shape at frequency 802.12 (Theoretical Analysis).

The mode shapes of experimental and theoretical analysis at the frequency 827.11 Hz and 802.12 Hz are similar respectively. The percentage error considering their frequencies has been calculated.

Percentage Error

$$\frac{827.11-802.12}{827.11} * 100\% = 3.021\%$$

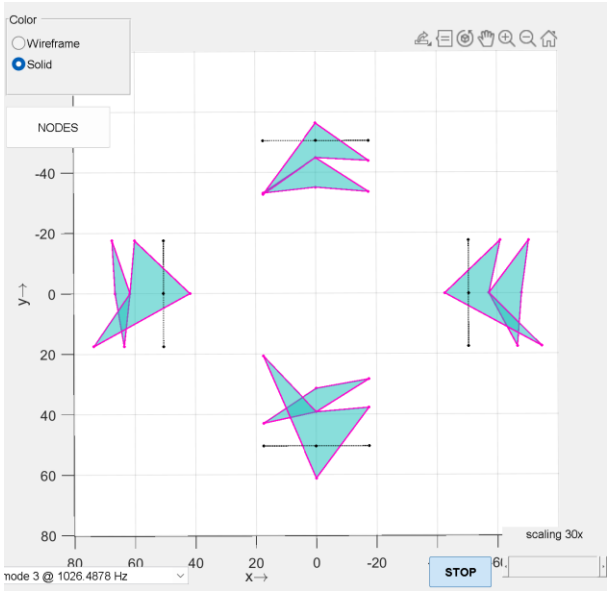

Figure 24.23:Modal shape at frequency 1026.48 Hz Hz. . (Experimental Analysis).

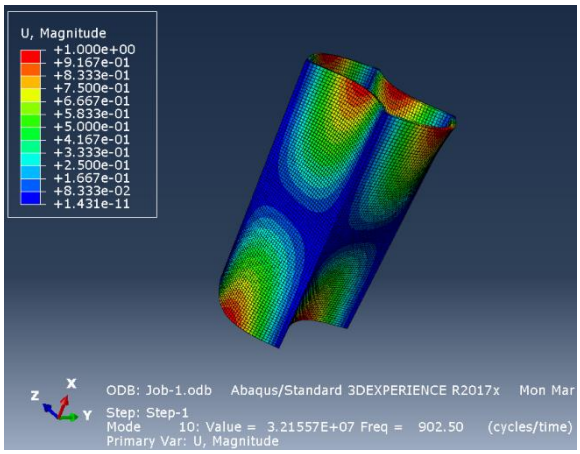

Figure 25.24:Mode shape at frequency 902.50 (Theoretical Analysis).

The mode shapes of experimental and theoretical analysis at the frequency 1026.48 Hz and 902.50 Hz are similar respectively. The percentage error considering their frequencies has been calculated.

Percentage Error

$$\frac{1026.48-902.50}{1026.48} * 100\% = 12.07\%$$

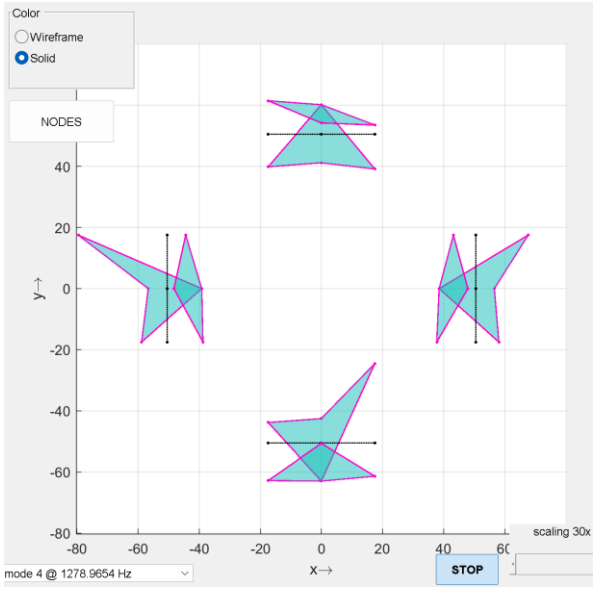

Figure 26.25: Modal shape at frequency 1278.96 Hz Hz. (Experimental Analysis).

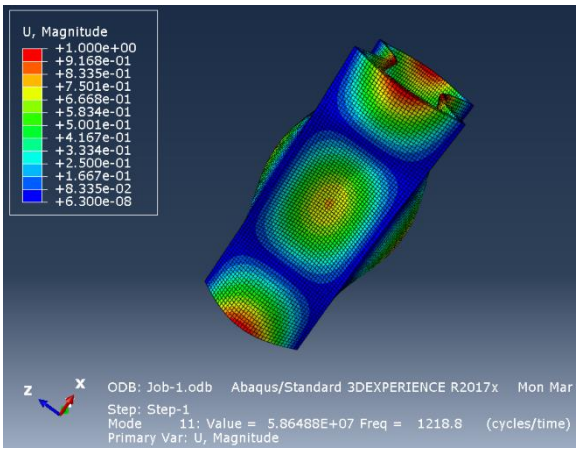

Figure 27.26: Mode shape at frequency 1218.8 (Theoretical Analysis).

The mode shapes of experimental and theoretical analysis at the frequency 1278.96 Hz and 1218.8 Hz are similar respectively. The percentage error considering their frequencies has been calculated.

Percentage Error

$$\frac{1278.96-1218.8}{1278.96} * 100\% = 4.70\%$$

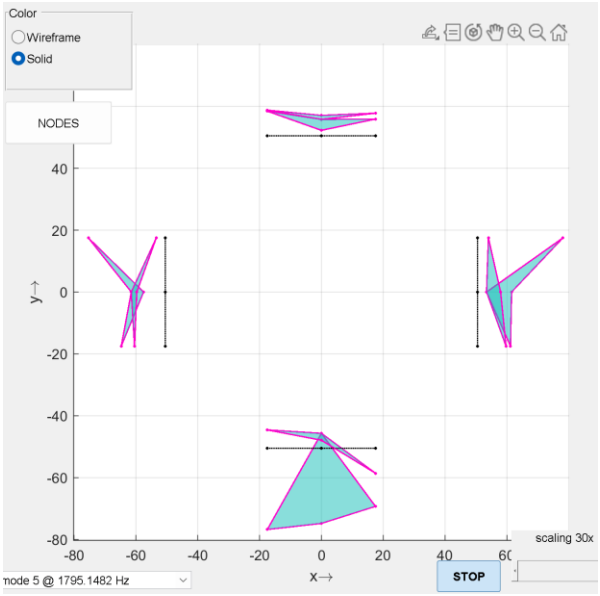

Figure 28.27: Modal shape at frequency 1795.14 Hz.). Hz. (Experimental Analysis)

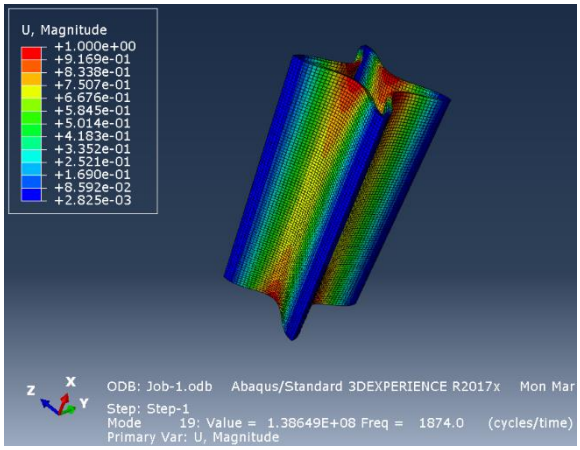

Figure 29.28: Mode shape at frequency 1874.0 (Theoretical Analysis).

The mode shapes of experimental and theoretical analysis at the frequency 1795.14 Hz and 1874.0 Hz are similar respectively. The percentage error considering their frequencies has been calculated.

Percentage Error

$$\frac{1874.0-1795.14}{1874.0} * 100\% = 4.20\%$$

The percentage error comparing some of the mode shapes with theoretical analysis is higher than 10% whereas some of the modes shapes has very less percentage error. These discrepancies between experiment and mathematical model are due to following reasons.

i. **Youngs Modulus:** Using the highest value of the Young's modulus of aluminium results in quite higher difference with the obtained frequencies from the experimental method whereas the lowest value of the Young's modulus result in closer frequency and modal shapes. It is because the exact material cannot be confirmed with its only one property i.e., only density of a material is used here to identify the material. Therefore, the actual material could be something else with different young's modulus. But, for this mathematical model, it is considered as aluminium **(R. Pintelon 1, Measurement of young's modulus via modal analysis experiments: a system identification approach, 2003).**

ii. The experiment was done in the prism which has a weld in the corners. The welding is infinitely rigid which cause stiffness loss in the corner. The loss of stiffness leads to decrease in the natural frequency, whereas the mathematical model is created with continuous hollow shape of the prism where there is no loss of stiffness resulting in the high frequencies **(Wilson, 2012).**

iii. Although the analysis was free-free, but the actual experiment was done hanging the prism in a bungee cord considering no boundary conditions has been applied but in some of the mode shapes, the top edge of the structure is pinched with the bungee cord resulting in asymmetricity.

iv. Due to factors like sensor noise, the environment, and calibration errors, experimental observations may contain measurement inaccuracies. The recorded natural frequencies may not be accurate as a result of these measurement errors, which could result in differences between the experimental and mathematical findings.

v. The actual structure contains small holes on each side and corner which has been neglected in the mathematical modal. Although the modal shapes don't get affected by it in the lower frequencies. There might be little change in the modal shapes as the higher frequency modal shapes are analysed.

vi. Manufacturing tolerances may result in minor variations between the actual physical structure and the mathematical model, which may lead to discrepancies between experimental and mathematical results.

MAC:

MAC (Modal Assurance Criterion Analysis) is the used in the modal shape analysis to compare and determine the similarities between two mode shapes and it gives the idea of quantitative assessment of how closely two mode forms are correlated. Generally, it is used to compare the mode shapes of experimental and theoretical model. The similar mode shapes have the value of 1 or 100% and the MAC value for a mode form compared to itself is also 1 or 100% whereas absolutely different mode shapes have the approximately 0 value.

The MAC cannot be a unit matrix due to the mass orthogonal nature of the modal vectors. Changes in the order of vectors in one set affect the MAC matrix, resulting in a permutation matrix-like structure. The MAC matrix only ensures consistency and is only suitable for pre-test mode pairing, It cannot determine validity, distinguish between systematic errors and local discrepancies, or determine the completeness or orthogonality of vectors.

The complex modal vector at each common node is basically normalised to determine the MAC value between two modes. Those vectors are represented as $\{\phi_A\}$ and $\{\phi_X\}$. The MAC matrix of resulting scalar is:

$$MAC(r,q) = \frac{\left|\{\varphi_A\}_r^T \{\varphi_X\}_q\right|^2}{\left(\{\varphi_A\}_r^T \{\varphi_A\}_r\right)\left(\{\varphi_X\}_q^T \{\varphi_X\}_q\right)}$$

Figure 30.29: MAC equation ***(Miroslav Pastor, 2012)***

In the case of prism with 28 nodes, the mode shape components at each of the 28 measured nodes are considered when calculating the MAC value, but the amplitude node with the greater locations will be given more importance **(Miroslav Pastor, 2012).**

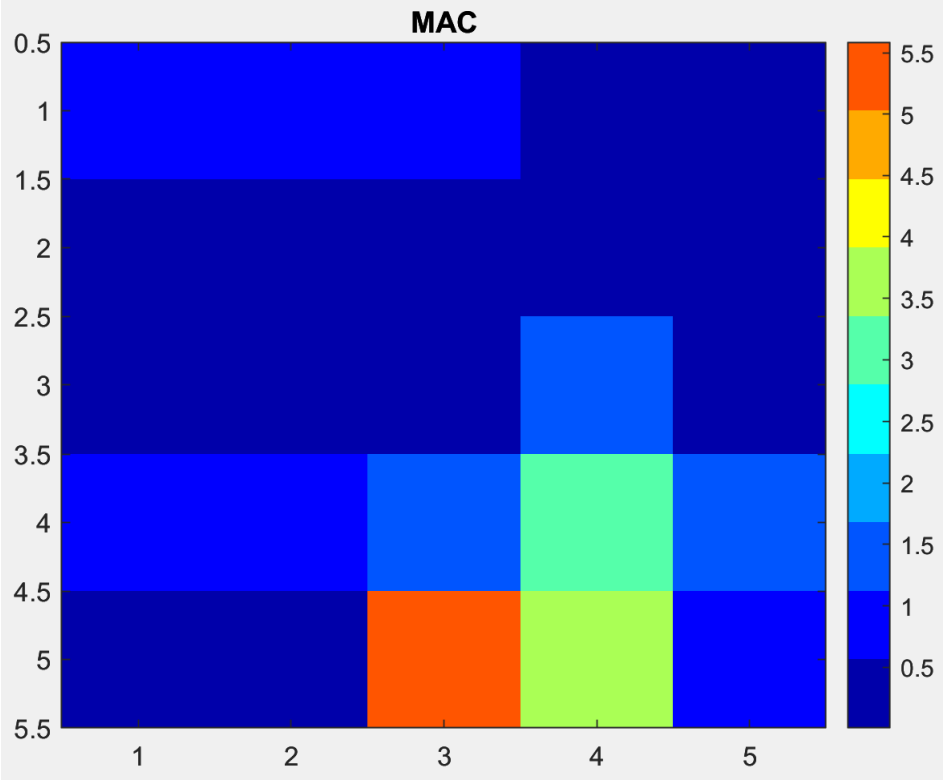

Figure 31.29: MAC comparison between mode shapes of experimental and theoretical analysis done for prism.

The MAC was utilized to compare the mode shapes between experimental and theoretical analysis. Since, the physical structure consists of 28 nodes, the magnitudes of those 28 nodes in the mathematical model were extracted using the co-ordinates of their location. The 5 modes shapes of the experimental analysis were compared with the 5 mode shapes of theoretical. Therefore, the [28x5] matrix was formed from the magnitudes extracted from the mathematical model and is compared with the magnitudes of the experimental model at the specific locations of each node. The result obtained was not satisfying as it doesn't reflect exact comparison between the mode shapes, and it is due to following reasons:

i. MAC is very sensitive as small variations in the mode shapes can cause significant changes in MAC value. This can be especially challenging when comparing mode shapes obtained from various measurement sources, such as experimental data and finite element analysis results, which can add sources of error and uncertainty. The same problem can be seen here as there are lots of discrepancies between experimental and theoretical modal which has already been mentioned resulting in incorrect MAC **(Miroslav Pastor, 2012).**
ii. Another reason could be the incorrect co-ordinate selection for the node location during mathematical analysis may result in the incorrect MAC.

COMAC

The Coordinate Modal Assurance Criterion (COMAC) is a MAC enhancement, that determines the areas of a structure that are subject to the low correlation of degrees of freedom. COMAC is computed when choosing a set of mode pairs, each pair comprised of two modal vectors having the same degree of freedom. This mode pair set contains all modes of interest within a specific frequency range. When comparing two sets of modes, a COMAC value for each measurement degree of freedom is computed.

Like MAC values, the range of values are 0 to 1 for COMAC, with 1 indicating perfect correlation between two complex mode shapes.

Assuming there is a match for every modal vector in the two sets, COMAC is computed after the mode pairs have been identified with MAC shown in the equation in figure XX. Furthermore, the modal vectors are renumbered to ensure that the corresponding modal vectors have the same subscript. *(Allemang, 2003)*

$$COMAC_q = \frac{\sum_{r=1}^{L} \left| \psi_{qr} \phi_{qr} \right|^2}{\sum_{r=1}^{L} \psi_{qr} \psi_{qr}^* \sum_{r=1}^{L} \psi_{qr} \psi_{qr}^*}$$

Figure 32.30:COMAC Equation (Allemang, 2003)

Frequency Response Assurance Criterion (FRAC)

Frequency Response Assurance Criterion (FRAC) measures the correlation between two frequency response functions representing the same input-output relationship by determining to which extent each degree-of-freedom contributes to a particular mode shape. The measured and synthesised FRFs are linearly related at all frequencies, which can be compared over a complete or partial frequency range. Similarly to MAC and COMAC, FRAC values range from 0 to 1, with 1 showing that a specific degree of freedom is fully involved in a specific mode shape and 0 indicating the inverse. Understanding the behaviour of a structure in this way provides the engineer with the knowledge needed to optimise the structure or spot potential areas of failure.

$$FRAC_{pq} = \frac{\left| \sum_{\omega=\omega_1}^{\omega_2} H_{pq}(\omega) H_{pq}^*(\omega) \right|^2}{\sum_{\omega=\omega_1}^{\omega_2} H_{pq}(\omega) H_{pq}^*(\omega) \sum_{\omega=\omega_1}^{\omega_2} H_{pq}(\omega) \hat{H}_{pq}^*(\omega)}$$

Figure 33.31:: FRAC equations (Allemang, 2003)

To reconcile discrepant results, The mathematical model can be amended in the following ways.

i. Sometimes discrepancies arise due to failure to recognise the material. Therefore, with thorough study, a material property like young's modulus can be adjusted to fit the physical structure more closely. This may entail conducting additional tests to measure the material properties or using more precise material data.
ii. Different damping processes, such as friction and material damping, cause energy to be lost in actual structures. The mathematical model can better capture the behaviour of the physical structure by including damping effects, leading to findings that are more consistent with experimental data.

iii. There is an effect of external factors such as temperature change, wind loads, noise which are neglected in the mathematical model, although this has negligible effect in a closed room with maintained temperature, but any changes can be considered in mathematical model to achieve precise result.

iv. Mesh convergence is necessary to achieve better result. Since, the ABAQUS software used for the mathematical analysis allows only certain number of nodes for the mesh, the fully converged mesh couldn't be achieved. Therefore, other professional software's can be used for the analysis.

v. The data used for the mathematical model was taken from the experiment done in the welded prism in the corners. Therefore, the welding might be used in the mathematical model using Abaqus Welding Interfaces to mimic the real physical structure.

vi. Although the experiment was free-free analysis, the bungee cord that was used to suspend the structure may have played a small part as a boundary condition that could also be taken into account in the mathematical model.

Concluding remarks:

The experimental and theoretical analysis was performed, and the modal shapes obtained from both methods were studied and compared. There were certain discrepancies found between the modal shapes obtained from experimental and theoretical analysis and some of the major reasons were due to the assumption of a material to be aluminium which was found using only one property of a material available i.e., density, not mimicking the actual welded structure of the prism used in experiment. Similarly, the MAC which was used to quantitively compare the modal shapes between experimental and theoretical analysis produced unexpected results and it was due to the sensitiveness of the MAC which made it challenging as the theoretical and experimental model already had lots of discrepancies. However, the learning objective was achieved and the amendments that needed to be done in the mathematical model to obtain the optimized result was learned.

References

Instruments., C. (2016, nd nd). *Basics of Modal Testing and Analysis*. Retrieved from Crystal Instruments.: https://www.crystalinstruments.com/basics-of-modal-testing-and-analysis

Jimin He, Z.-F. F. (nd, nd nd). *Overview of modal analysis*. Retrieved from ScienceDirect.:

MathWorks. (n.d.). *MathWorks*. Retrieved from modalsd: https://uk.mathworks.com/help/signal/ref/modalsd.html

MathWorks. (n.d.). *modalfrf*. Retrieved from MathWorks: https://uk.mathworks.com/help/signal/ref/modalfrf.html

Miroslav Pastor, M. B. (2012). Modal Assurance Criterion. *ScienceDirect*, 5.

R. Pintelon 1, P. G. (2003). Measurement of young's modulus via modal analysis experiments: a system identification approach. *ScienceDirect*, 5. Retrieved from Measurement of young's modulus via modal analysis experiments: a system identification approach.

R. Pintelon 1, P. G. (2012). *Welded Frame Finite ElementModelling and Experimental Modelling Analysis.* R. Pintelon 1, P. Guillaume 2, K. De Belder 1, Y. Rolain 1: Blekinge Tekniska Hogskola.

Wilson, M. K. (2012). *Welded Frame Finite ElementModelling and Experimental Modelling Analysis.* R. Pintelon 1, P. Guillaume 2, K. De Belder 1, Y. Rolain 1: Blekinge Tekniska Hogskola.